Three-Dimensional Image Analysis of Mixing in Stirred Vessels

Lin Li and James Wei
School of Engineering and Applied Science, Princeton University, Princeton, NJ 08544

Several analytical methods were applied to the 3-D electrical resistance tomography (ERT) image of stirred-vessel experiments of Holden et al. to characterize the mixing behavior and to measure mixing quantitatively. Based on the time resolved 3-D ERT results, the centroid and variance of the concentration distribution in three dimensions can be obtained as a time series to track the movement, dispersion, stretch and rotation of the concentration distribution in the tank. By sampling at different scales and locations, the ratios of standard deviations to means and the entropy of corresponding volumes can be calculated to examine the degrees of uniformity. The 3-D wavelet decomposition provides an effective method of analyzing the mixing process at various scales. The wavelet difference coefficients reflect the concentration gradients of specific volumes along different directions. These methods of analysis promise to guide the design of better mixing schemes and to monitor the process for optimal operation.

Introduction

Research in mixing has emphasized the input process such as: the shape and number of the turbine blades, the position and width of the baffles, the horsepower per gallon of input power, and the duration of mixing (Nagatam, 1975; Oldshue, 1983; Ranz, 1985; Ottino, 1989). A complementary outcome analysis should address the questions: How do you measure the uniformity of the mixture?; How do you know when the mixture is uniform enough? When is the best time to stop the mixing process?; and How do you know that you are using the right mixing equipment? For example, de la Villeon et al. (1998) used several criteria to study the stirring efficiency of three helical ribbon impellers, including the standard deviation of concentration to characterize the dispersion of clustered tracers, the length stretch to quantity the amount of stretching that can be generated by the impeller, and the dispersive mixing efficiency coefficient to measure the relative importance of extension effects over the rotational effects in a flow.

We propose to analyze data from 3-D time-dependent mixing, such as by following the concentrations at various parts of the equipment with time (Danckwerts, 1981) with the following measures:

(a) Tracking the centroid, dispersion, stretch and rotation of concentration distributions in three dimensions

(b) Analyzing sample concentration distributions to compute the ratios of standard deviation to mean, and the entropy

(c) Wavelet analysis of concentration averages and gradients in different directions, by multiple scales in three-dimensions.

The technology for 3-D imaging has produced a revolution in our understanding of medicine (Jain, 1989; Russ, 1994). We now have the capability of producing 3-D measurements with time resolution, such as the recent work of Holden et al. (1998), which makes measurements of electrical resistance tomography (ERT) in a 2.7-m^3 stirred tank (1.43 m in diameter; 1.695 m in height) with the injection of a slug of 1 L of concentrated salt solution into a tank of tap water. The result is measurements of concentrations in the rectangular axes with time, and the data is available as a stack of 8 horizontal planes, each plane has 316 voxels (volume elements), so that there are $316 \times 8 = 2{,}528$ voxels. Each voxel represents a vol-

Correspondence concerning this article should be addressed to J. Wei.

ume of 71.5 mm × 71.5 mm × 165 mm or 0.843 L. The conductivity of a voxel is measured as $C(x, y, z, t)$, where the conductivity range from 109 to 318 (highest). The concentration should be roughly in proportion to the conductivity.

The Holden's data was obtained with two different types of stirrers: the Rushton disk turbine with six flat blades that produce primarily a radial thrust at mid-level; and the Lightnin A310 with propeller blades that produce an axial downflow. They were both stirred at the rate of 75 revolutions per min, without baffles.

A sample of the Holden data is shown in Figure 1 as a stack of eight 3-D plots of concentration vs. x (from 1 on the left to 20 on the right) and y (from 1 in the front to 20 in the back), each plot represents a horizontal plane with the coor-

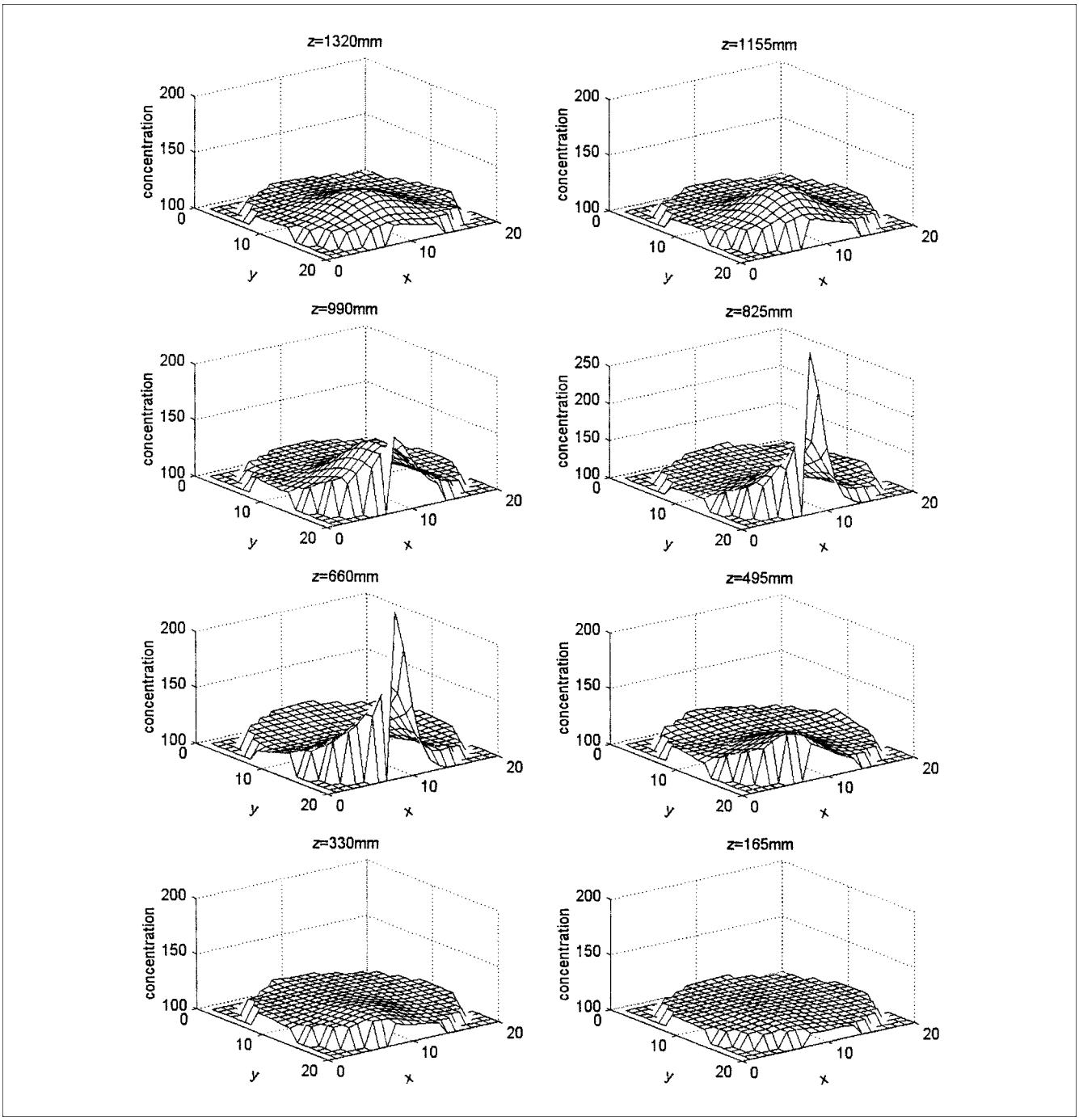

Figure 1. Electrical resistance tomography measurements of Rushton mixer at $t = 4$ seconds after injection of salt solution.

The x axis has 20 levels from 1 (left) to 20 (right); the y axis has 20 levels from 1 (back) to 20 (front). The eight figures represent the eight vertical levels. The conductivity C has a minimum level of 109 (pure water) to 318 (highest salt solution).

dinates of z. ($z = 0$ represents the bottom of the tank, so the eight planes are located from $z = 165$ to 1320 mm with equal thickness of 165 mm.) This figure represents the measurements with the Rushton turbine at $t = 4$ s after the injection of a liter of salt solution near the top center at a position of $x = 15$, $y = 15$, and $z = 1320$ mm. It is readily seen that the maximum concentration has moved down to planes of $z = 660$ mm and 825 mm on the wall and in the direction pointing south ($x = 8$, $y = 20$).

Tracking the Centroid, Dispersion, Stretch and Rotation

This set of data is more conveniently transformed into cylindrical coordinates $C(r, \theta, z, t)$, of $16 \times 80 \times 8 = 10{,}240$ voxels. Here the size of the voxel in the radial direction is $(1.43/2)/16 = 44.7$ mm in the angular direction is $2\pi/80 = 0.0785$ radiant, and in the vertical direction is 165 mm. A voxel will vary in volume from the smallest at the center to the largest next to the wall, as $r = 45$ to 715 mm, so that the voxel volume varies from 25.9 to 413.9 mL, but the average is 208 mL. When this set of concentrations in Figure 1 is transformed into cylindrical coordinates, the results are shown in Figure 2 as a stack of 3-D plots of concentration vs. r from 0 (center) to 715 mm (wall), and θ from 1 to 360° (θ increases clockwise with $\theta = 0$ represents the north). Due to volume averaging in the coordinate transformation, the maximum concentration attained is 199, which is attained $z = 825$ mm, and with the parameter values of $r = 715$ mm and $\theta = 193.5°$. Hereafter, the concentration will be expressed as normalized conductivity

$$c = \frac{C - \min(C)}{\max(C) - \min(C)}$$

There is a great deal of data to keep track of, especially when presenting a times series. We should begin by tracking the ''center of mass'' and the ''standard deviations'' of the concentration distribution in three dimensions (Danckwerts, 1981). The concentration centroid is defined by the coordinates

$$\langle r \rangle(t) \equiv \int rc(d\upsilon) \Big/ \int c(d\upsilon)$$

$$\langle \theta \rangle(t) \equiv \int \theta c(d\upsilon) \Big/ \int c(d\upsilon)$$

$$\langle z \rangle(t) \equiv \int zc(d\upsilon) \Big/ \int c(d\upsilon)$$

$$\sigma_r^2(t) \equiv \int (r - \langle r \rangle)^2 c(d\upsilon) \Big/ \int c(d\upsilon)$$

$$\sigma_\theta^2(t) \equiv \int (\theta - \langle \theta \rangle)^2 c(d\upsilon) \Big/ \int c(d\upsilon)$$

$$\sigma_z^2(t) \equiv \int (z - \langle z \rangle)^2 c(d\upsilon) \Big/ \int c(d\upsilon)$$

The three terms $\langle r \rangle$, $\langle \theta \rangle$, and $\langle z \rangle$ define the position of the centroid or the average concentration in the tank, which describes the circulation from the point of the injection. The three terms σ_θ, σ_r, σ_z, describe the dispersion of the salt from the position of the concentration centroid. A good mixing scheme should have a good circulation rate and a fast dispersion rate.

Figure 3 shows a comparison of the Rushton and the Lightnin mixer results. The radial position of the centroid $\langle r \rangle$ in the Rushton mixer moves from the position of 379 mm at $t = 2$ s outward, and converges to the average position of 492 mm in about 15 s; however, it takes about 30 s for the Lightnin mixer. The angular position $\langle \theta \rangle$ of Rushton result takes a clockwise motion from 170° to a maximum of 228°, then comes back to the steady-state value of 180°. For Lightnin, result $\langle \theta \rangle$ increases from 160° to a maximum of 204°, then converges to the steady state gradually. The vertical position of the centroid $\langle z \rangle$ in the Rushton result converges to the steady-state value of 734 mm in 15 s, but it takes 30 s in the Lightnin. In the examination of dispersion, rotation and stretch, it is more convenient to return to the Cartesian coordinates

$$V_{xx} = \int (x - \langle x \rangle)^2 c d\upsilon \Big/ \int c d\upsilon$$

$$V_{xy} = \int (x - \langle x \rangle)(y - \langle y \rangle) c d\upsilon \Big/ \int c d\upsilon$$

The variance matrix V is given as

$$\begin{bmatrix} V_{xx} & V_{xy} & V_{xz} \\ V_{xy} & V_{yy} & V_{yz} \\ V_{xz} & V_{yz} & V_{zz} \end{bmatrix}$$

The square root of the trace $\sigma = \sqrt{V_{xx}^2 + V_{yy}^2 + V_{zz}^2}$ is the average dispersion for the concentration distribution. When the V matrix is diagonalized, the eigenvectors give the rotation angles of the principle axes, and the eigenvalues give the variances along these axes. The rotation can be quantified by the angle θ, which is in a clockwise rotation around the z axis, measuring from north as zero, and the angle ϕ, which is the angle above the x-y plane. When we arrange the square roots of the eigenvalues in the order $\lambda_3 > \lambda_2 > \lambda_1$, the ratio λ_3/λ_1 gives the stretch which is the ratio of the largest to the smallest dispersion. For the Rushton mixer, Figure 4a gives a plot of the dispersion σ, which goes from 360 to 630 mm, and the stretch λ_3/λ_1, which goes from a maximum of 1.5 to 1 (isotropic) vs. time; and Figure 4b gives the major axis angle θ, which goes from 210° to 15°, and ϕ, which goes from 30 up to the zenith at 90, and passes it to 105°. At this degree of resolution ($\Delta x = \Delta y = 71$ mm, $\Delta z = 165$ mm, $\Delta t = 2$ s), much of the work of the stirrer in stretching of the fluid is lost by volume and time averaging. When measurement techniques advance to the point of 1 mm and 1 ms resolution, we can look forward to larger degrees of detail.

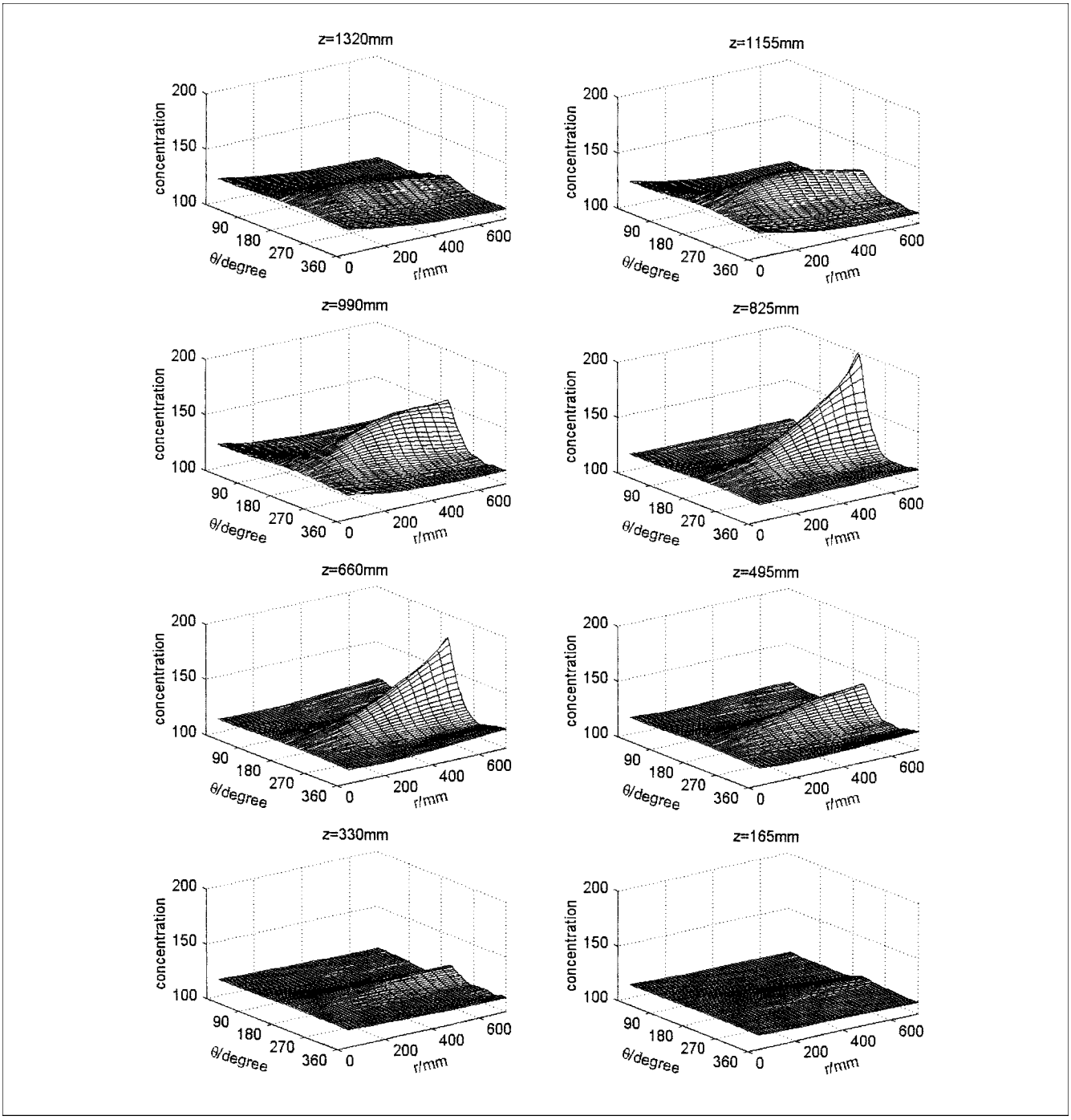

Figure 2. ERT results of Figure 1 in cylindrical coordinates.

Sample Concentration Distributions, Standard Deviation and Entropy as Instantaneous Status and as Time Series

It is an intuitive idea that a mixture is uniform if samples at different locations yield the same concentration. This can be formalized by dividing the volume into a number of cells, and measure the concentration of each cell to obtain a sample distribution. Two of the more obvious measures are the ratio of the standard deviation to mean, and the entropy (Jain, 1989). They can be defined as

$$\langle c \rangle = m \equiv \int c dv \Big/ \int dv$$

$$\sigma_c^2 \equiv \int (c - m)^2 dv \Big/ \int dv$$

$$S \equiv - \int c \cdot \ln(c) dv$$

For a perfect mixture, the standard deviation is zero and the entropy is at maximum. For a completely segregated mix-

ture where all concentration is in one cell, the standard deviation is as a maximum and the entropy is zero.

Let us look at the concentration as a time-series to see the rate of approach to uniformity. It is difficult to make sense of a set of $16\times80\times8=10{,}240$ voxels as a function of time, and it would be easier to make progress by making an average of all the concentrations at the same horizontal plane, so that we have

$$c_z = \int\int c(d\theta)(rdr) \Big/ \int\int (d\theta)(rdr)$$

$$\sigma_{cz}^2 = \int\int (c-c_z)^2(d\theta)(rdr) \Big/ \int\int (d\theta)(rdr)$$

Figure 5 gives the results for Rushton stirrer, which shows the mean value c_z, the ratio of standard deviation to mean σ_{cz}/c_z, and the entropy S. The eight lines represent the eight vertical levels from the hot color of top plane at $z=1{,}320$ mm to the cold color of the bottom plane at $z=165$ mm. Figure 6 represents the same results for the Lightnin stirrer.

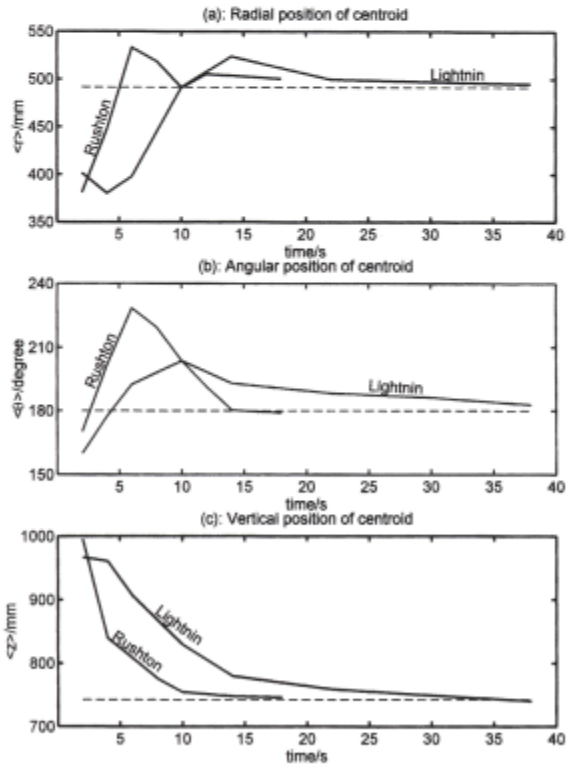

Figure 3. Three measures of the center of mass of the concentration distribution: Rushton vs. Lightnin.

(a) $\langle r\rangle$ measures the radial position; (b) $\langle\theta\rangle$ measures the angular position; and (c) $\langle z\rangle$ measures the vertical position.

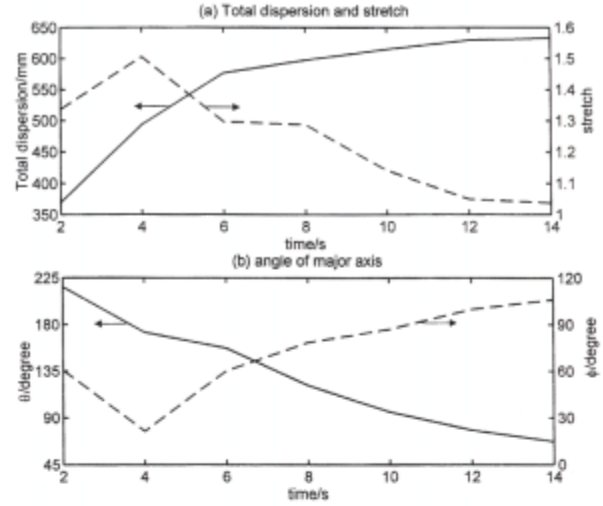

Figure 4. Dispersion analysis of the Rushton mixer.

(a) Total dispersion and the stretch vs. time; (b) the rotation measured in the angle θ in the clockwise direction from the x axis and around the z axis, and the angle ϕ above the x-y plane.

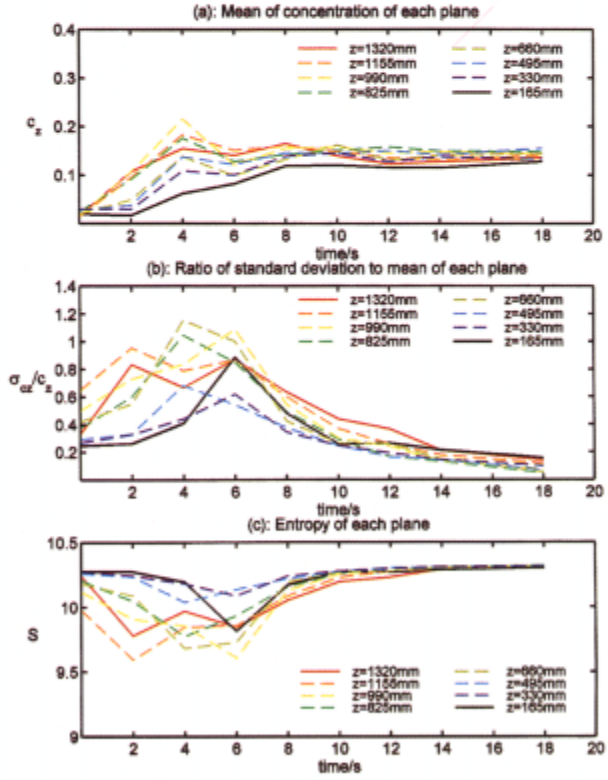

Figure 5. Normalized conductivity, standard deviation/conductivity, and entropy vs. time for Rushton.

(a) Mean conductivity averaged over z planes vs. time. The eight lines represent the eight vertical or z levels; (b) the standard deviation divided by average over z planes; (c) the entropy over z planes.

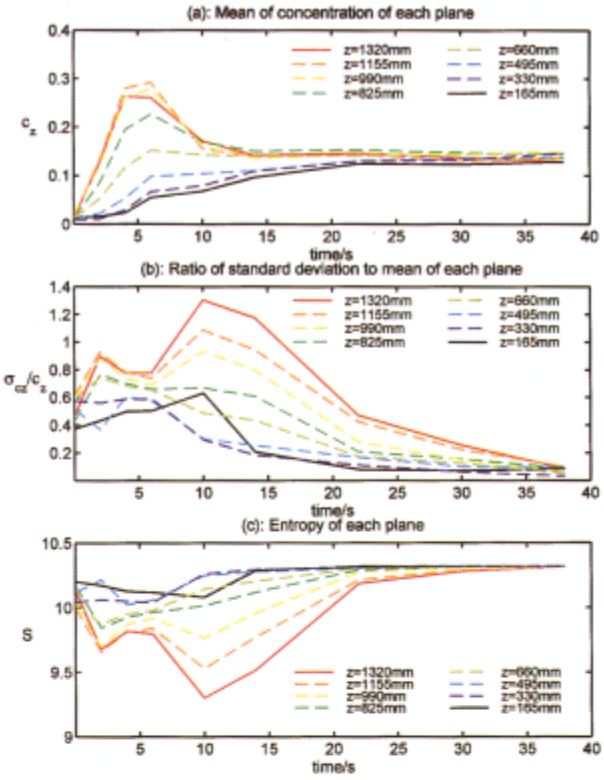

Figure 6. Normalized conductivity, standard deviation/ conductivity, and entropy vs. time for Lightnin.

Let us first examine the mean value of each plane c_z. If the concentrations are linear to the conductivities, and, if there is a mass conservation, then the average of these eight measurements should remain constant. This is not the case, and in Figure 5 there is a rise from $t = 2$ s to $t = 8$ s before it levels off. It is probable that when the concentrations are very nonuniform within a voxel, the measured conductivity is not simply a volume average, so we have to use the early time results with caution.

It is seen that for the Rushton stirrer, there is only a small vertical variation c_z among these eight horizontal levels, which indicates a good vertical mixing. The position of maximum concentration began at the top plane of the tank, then descended to level 990 and 825 mm at $t = 4$ s, and then returned to the top plane of $z = 1{,}320$ mm at $t = 6$ s. This indicates that the injected salt slug was pulled down to mid-level by the circulation cell, and then returned to the top plane by the cell. On the other hand, there is considerably more vertical variation in the Lightnin run, where the maximum concentration remains at the top planes of the tank throughout the period, and the minimum concentration remains at the bottom plane. The injected salt slug stayed at the top, and never traveled downwards, which is a major failure. If we measure of the rate of approach to uniformity by the time it takes to reach 90% uniformity, it is seen that the Rushton run requires about 8 s, and the Lightnin run requires about 14 s.

We examine next the degree of uniformity within each plane by looking at the ratio of standard deviation to mean, and by looking at entropy. The rate of convergence to a steady-state value is faster for entropy than for σ_{cz}/c_z, as entropy is a less demanding measure of uniformity than σ_{cz}/c_z or σ/m. For the Rushton run, the maximum value for σ/m occurs in the top levels at 2 s, and moves to the mid levels as $t = 4$ to 6 s, then return to the top levels at higher times. The approach to uniformity is 90% complete at around 12 s. For the Lightnin, the maximum value for σ/m remained at top through the run, and the minimum value remained at the bottom. The approach to uniformity is delayed to around 30 s.

Wavelet Multiscale Analysis as Instantaneous Status and as Time Series

Digital image processing is the art and science of analyzing image information, in fields ranging from remote sensing by satellites, to astronomy, radar and sonar, medical diagnosis, and photography (Daubechies, 1991; Strang and Nyuyen, 1997). The Fourier transformation is a favorite method to analyze a signal, and to break it down to the sum of a number of sinusoidal elements. Given a function $f(x)$ with a period L, its Discrete Fourier Transform coefficients are a_k and b_k, so that the reconstructed function f is given by

$$f(x) = a_0 + \Sigma a_k \cos(k\omega x) + b_k \sin(k\omega x)$$

where ω is the fundamental frequency $2\pi/L$. Since k represents the natural numbers 1, 2, 3, ..., n, the wave lengths of the elements are $L/1$, $L/2$, $L/3$, ..., L/n. For a detailed analysis using many elements, such as n going up to 64, its loss of effectiveness as a wave of length $L/63$ is almost indistinguishable from a wave of length $L/64$. Knowing the value of the coefficient a_{64} also does not help you to locate the position of the maximum of the wave. The wavelets are a major advance from Fourier series in multiscale analysis, as it represents the function $f(x)$ with one wave of length L, two of wave length $L/2$, four of $L/4$, eight of $L/8$, sixteen of $L/16$, and so on. Knowing the value of a coefficient will also tell you precisely where is the position of the wave. A full discussion of 3-D wavelet analysis is given in Wei (1999), and a brief discussion is given here. Let us begin to introduce the terminologies of wavelet analysis by considering a 1-D signal divided into a discrete series of cells

$f1$	$f2$	$f3$	$f4$	$f5$	$f6$	$f7$	$f8$

The first level of wavelet analysis by the Haar function begins by creating two sets of coefficients:
Approximation coefficient

$$cA1 = (f1 + f2, f3 + f4, f5 + f6, f7 + f8)/\sqrt{2}$$

Difference coefficient

$$cD1 = (f1 - f2, f3 - f4, f5 - f6, f7 - f8)/\sqrt{2}$$

The first set is the approximation coefficients which measure the average of two cells at a time, and the second set is the difference coefficient, which measures the difference or gradient of two cells at a time. The first level of analysis concentrates on a short wave length of two cells, and gives a fine scale detail.

When we go to second level of wavelet analysis, we create

$$cA2 = (f1 + f2 + f3 + f4, f5 + f6 + f7 + f8)/2$$

$$cD2 = (f1 + f2 - f3 - f4, f5 + f6 - f7 - f8)/2$$

Now we are dealing with four cells at a time, and are describing the situation at a larger wavelength of four cells.

At the third level of analysis, we go to the longer wave of eight cells with

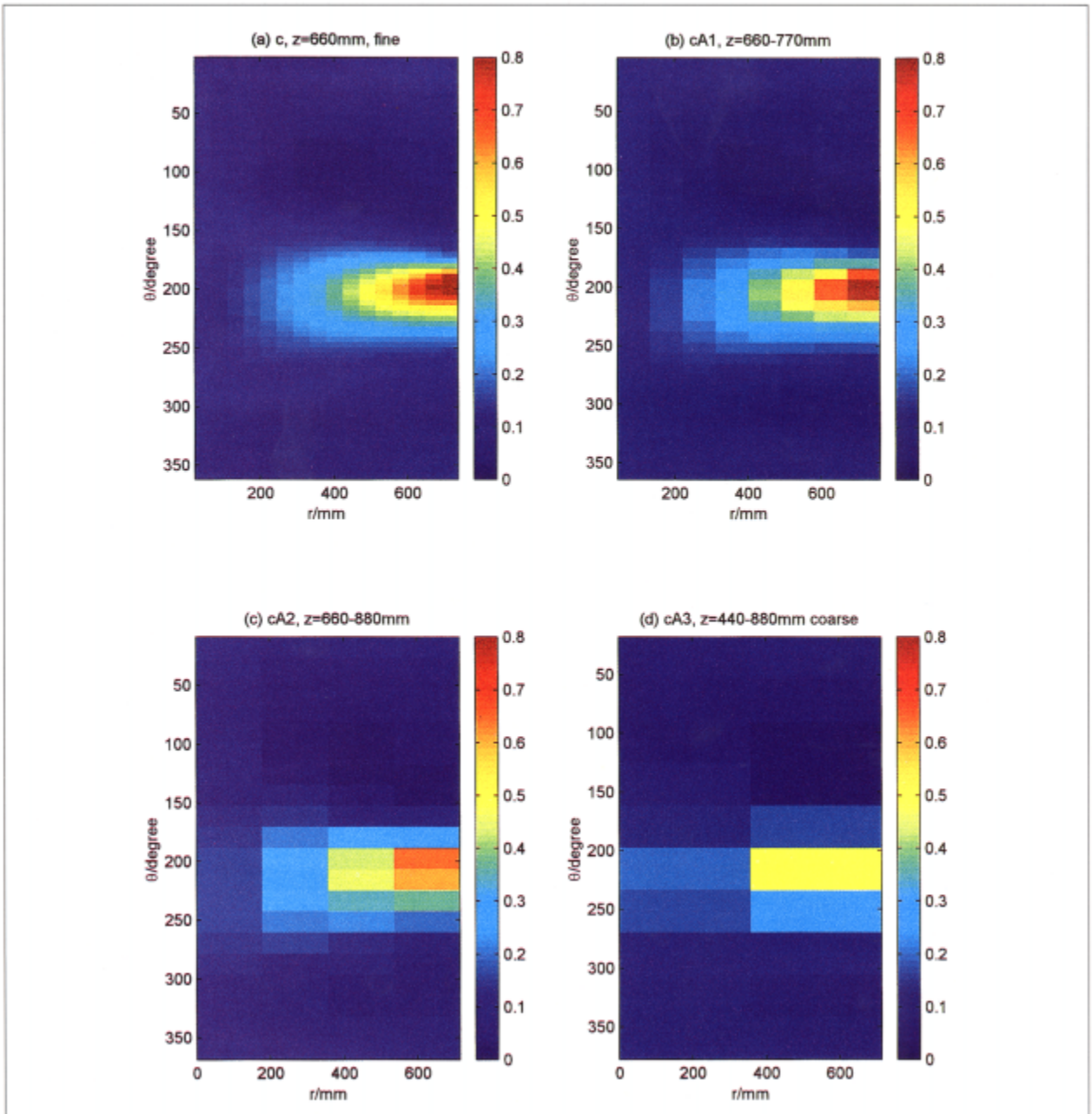

Figure 7. Wavelet analysis of the average functions of Rushton mixer at mid level and 4 s.

There are four levels of resolution from the finest detail to the broadest features: (a) the original conductivity data in 16×80 pixels at $z = 660$ mm; (b) the approximation coefficient cA1 in 8×40 pixels at $z = 660-770$ mm; (c) the approximation coefficient cA2 in 4×20 pixels at $z = 660-880$ mm; (d) the approximation coefficient cA3 in 2×10 pixels, at $z = 440-880$ mm.

$$cA3 = (f1 + f2 + f3 + f4 + f5 + f6 + f7 + f8)/\sqrt{8}$$

$$cD3 = (f1 + f2 + f3 + f4 - f5 - f6 - f7 - f8)/\sqrt{8}$$

This gives more of the "big picture," which may be familiar as the "thumbnail sketch" of the entire picture.

Let us give an example here. If f is a vector of (1, 2, 3, 4, 5, 6, 7, 8), then

$$cA1 = (3, 7, 11, 15)/\sqrt{2}$$

$$cD1 = (-1, -1, -1, -1)/\sqrt{2}$$

$$cA2 = (10, 26)/2$$

$$cD2 = (-4, -4)/2$$

$$cA3 = 36/\sqrt{8}$$

$$cD3 = -16/\sqrt{8}$$

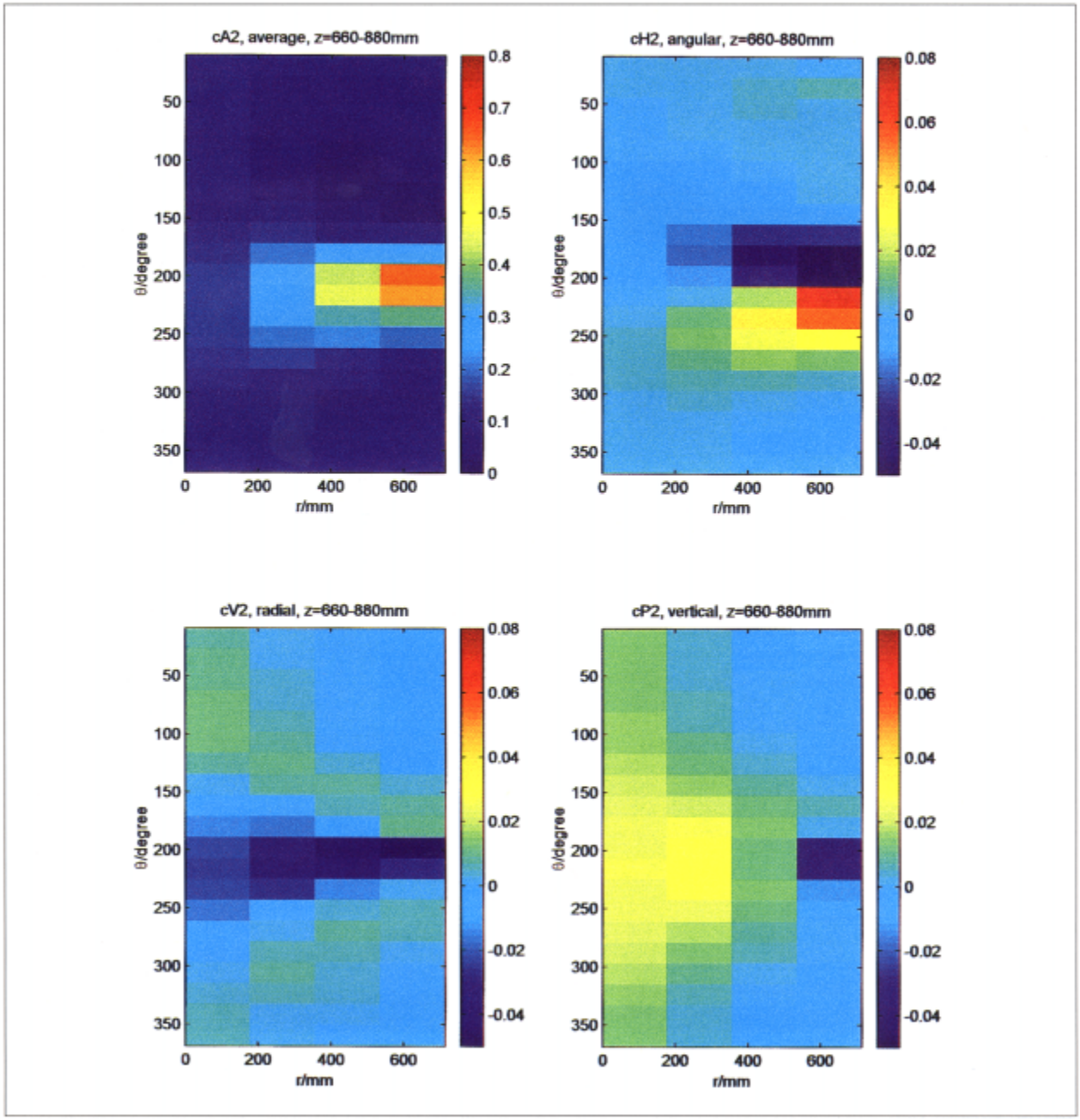

Figure 8. Wavelet analysis of Figure 7 showing the average and three gradients.

(a) cA2 is the same as Figure 7c; (b) the angular gradient cH2 which shows the counter-clockwise gradient; (c) the radial gradient cV2 from the wall to the center; (d) the vertical gradient cP2 which is from the bottom to the top.

Let us now advance to a 3-D signal set (Wei, 1999). There will be an average function cAn, but instead of a single difference function cDn between the left and the right, we will have seven difference functions. For discussing the uniformity of a mixture, three of them would be most important. In a cylindrical coordinate, these three difference coefficients are: cV: the Radial difference, from the center of the cylinder to the wall; cH: the angular difference, clockwise from north to east to south, to west; and cP: the vertical difference, from the top to the bottom.

Consider a set of measurements in a cubic set of $2\times2\times2$ cells. The coefficient cA1 is the average of the eight measurements; the coefficient cV1 is the difference between the left four cells and the right four cells; the coefficient cH1 is the

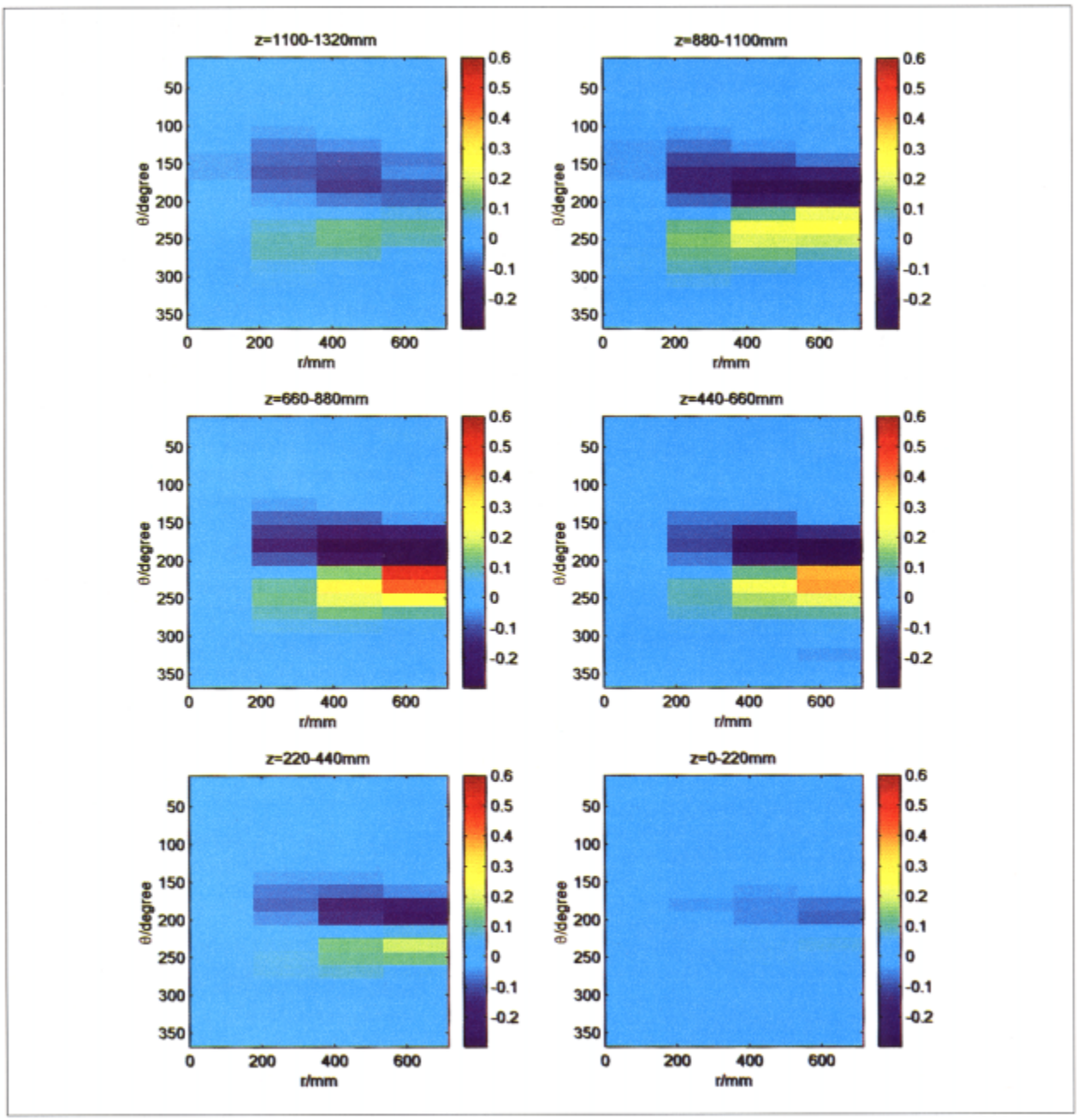

Figure 9. Wavelet analysis of Figure 7 showing the angular gradient cH2.

The six figures represent each of the 6 z level.

Table 1. Multilevel Wavelet Coefficients

Level	Avg.	Radial Gradient	Angular Gradient	Vertical Gradient
1 (Fine)	cA1	cV1	cH1	cP1
2	cA2	cV2	cH2	cP2
3	cA3	cV3	cH3	cP3
...	...	...	...	...
n (Broad)	cAn	cVn	cHn	cPn

difference between back four cells and the front four cells; and cP1 is the difference between the top four cells and the bottom four cells.

The entire set of analysis is shown in Table 1. After conversion to cylindrical coordinates, the ERT mixing results are expressed as $16\times80\times8$ 3-D matrices. In order to make the matrix size more suitable for wavelet analysis and voxel sizes along three directions which are approximately the same, we perform linear interpolation along the axial direction to convert the 3-D conductivity distribution into a $16\times80\times24$ matrix. For 3-D wavelet analysis, the wavelet coefficients cA, cH, cV, and cP, are also 3-D matrices. Here we give the data at specific z level to show the effect of the changing of the level from the original picture with $16\times80\times24$ voxels to the first level approximation cA1 with $8\times40\times12$ voxels, to the second level approximation cA2 with $4\times20\times6$ voxels, and, finally, to the third level approximation cA3 with $2\times10\times3$ voxels. See Figure 7, which represents the Rushton result at 4 s, and z at the mid-level. It should be indicated that for original data, each page of the 3-D conductivity matrix represents concentration distribution at the specific z position. However, for wavelet analysis results, each page of the 3-D coefficient matrix corresponds to a range in the z direction. For example, $c(i,j,12)$ represents the conductivity distribution at $z=660$ mm, but $\mathrm{cA1}(i,j,6)$ represents the average in the range of $z=660$ to 770 mm, $\mathrm{cA2}(i,j,3)$ represents the average in the range of $z=660$ to 880 mm, and $\mathrm{cA3}(i,j,2)$ represents the average in the range of $z=440$ to 880 mm, as shown in Figure 7. The picture of cA3 shows only the broad features, and gives a thumbnail sketch of the original picture. The picture of cA1 shows many more fine details.

In Figure 8 we give a set of wavelet analysis to show the entire average and gradients at the second level of analysis with $4\times20\times6$ voxels: the average cA2, the angular gradient cH2, the radial gradient cV2, and the vertical gradient cP2. This figure presents the Rushton result at $t=4$ s and z at the mid-level. The positive value of cH2 means concentration decreasing in the clockwise direction, and a negative value means concentration increasing. This set of pictures gives a diagnostic on where the nonhomogeneous regions are, which need attention.

Next we show a set of angular gradient cH2 for all six levels of z, as in Figure 9. It is clear that the two mid-z levels have much higher degree of angular gradient than the top and bottom levels, and they mainly occur at $\theta=230°$ and $r=700$ mm. Finally, we give the results of wavelet analysis as a time series in Figure 10. The difference coefficients cH, cV, and cP represent the concentration gradient along the angular, radial, and vertical direction, respectively. Therefore, we may use the absolute value of difference wavelet coefficients

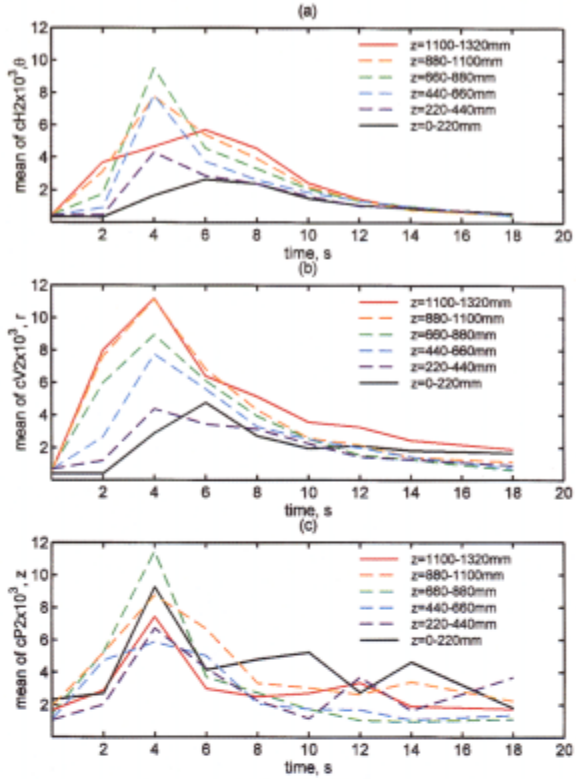

Figure 10. Wavelet analysis of Figure 7 showing the z plane averaged absolute values of cH2, cV2, cP2 vs. time.

The six lines represent the z levels.

as the measures of local homogeneity along specific direction. There are too many numbers to display, and we resort to averaging the absolute value of coefficients cH2, cV2, and cP2 over each plane to obtain $(\mathrm{cH2})_z$, $(\mathrm{cV2})_z$ and $(\mathrm{cP2})_z$. Figure 10 shows the values of $(\mathrm{cV2})_z$, $(\mathrm{cH2})_z$, and $(\mathrm{cP2})_z$ vs. time as six lines, representing all the z planes, from hot colors for the top of the tank to the cold colors at the bottom. This set of figures tells us how the nonhomogeneities are decaying with time. The largest radial gradients occur at the top level of z all the times, but the largest angular gradient was seized briefly by the midlevels at $t=4$, and the greatest vertical gradients are in the mid and bottom levels.

Conclusion

The time resolved 3-D ERT images can be analyzed to provide the centroid of the concentration distribution in the cylindrical coordinate axes of $\langle c\rangle=f(r,\theta,z)$, as well as the dispersions, stretch and rotation in the Cartesian axes of x, y, and z. We found that in the Rushton mixer, the centroid $\langle c\rangle$ approaches the steady-state value much faster than in the Lightnin mixer when they both operate at the same 75 rpm. However, the Rushton mixer uses nine times more power than the Lightnin. We can track the dispersion, stretch and rotation of the concentration distributions with time. We need finer and faster measurements to discover the detailed work of the stirrer to stretch and to rotate the fluid.

Table 2. Wavelet Coefficients for the Mixing Tank

Scale	Avg. Value	Center-Wall Diff.	Angular Diff.	Top-Bottom Diff.
Small, 110 mm	CA1	cV1	cH1	cP1
Medium, 220 mm	CA2	cV2	cH2	cP2
Large, 440 mm	CA3	cV3	cH3	cP3

The details of the structure of uniformity can be revealed by an analysis based on sample distribution. We distinguish between macro-uniformity, where the samples have large volumes, and micro-uniformity, where the samples have small volumes. Micro-uniformity is much more difficult to achieve than macro-uniformity. The ratio of standard deviation over the mean is a more demanding measure of uniformity than the entropy. When the rate of approach to uniformity is measured by the parameter σ/m, we found that at same rpm, Rushton mixer has a decided advantage over the Lightnin.

The wavelet analysis can give multiscale analysis of the structure of uniformity, which is useful in diagnosis on the problems encountered. A 3-D array of voxels are analyzed to obtain the average concentration (A), the radial gradient between the center and the wall (V), the angular gradient in a counter-clockwise direction (H), and the vertical gradient between top and the bottom (P). The scale of the array of voxels employed range from level one for fine detail (110 mm in *z*-direction) to level two for medium scale details (220 mm), and to level three for large scale features (440 mm). The results analyzed can be organized by the array shown in Table 2.

This multiscale diagnostic can be very useful in determining the properties of the mixer used, and the state of the mixture.

Acknowledgment

The authors are grateful to Holden and Mann for providing the original electrical resistance tomography disc, and to Mobil for financial support.

Literature Cited

Danckwerts, P. V., ''Mixture and Mixing,'' *Insights into Chemical Engineering*, Section E, Pergamon Press, New York, p. 256 (1981).

Daubechies, I., *Ten Lectures on Wavelets*, Society of Industrial and Applied Mathematics, Philadelphia (1991).

de la Villeon, F. Bertrand, P. A. Tanguy, R. Labrie, J. Bousquet, and D. Lebouvier, ''Numerical Investigation of Mixing Efficiency of Helical Ribbons,'' *AIChE J.*, **44**, 972 (1998).

Holden, P. J., M. Wang, R. Mann, F. J. Pickin, and R. B. Edwards, ''Imaging Stirred-Vessel Macromixing Using Electrical Resistance Tomography,'' *AIChE J.*, **44**, 780 (1998).

Jain, A. K., *Fundamentals of Digital Image Processing*, Prentice Hall, New York (1989).

Nagatam, S., *Mixing: Principles and Applications*, Wiley, New York (1975).

Oldshue, J. Y., *Fluid Mixing Technology*, McGraw-Hill, New York (1983).

Ottino, J. M., *The Kinematics of Mixing: Stretching, Chaos, and Transport*, Cambridge Univ. Press, Cambridge (1989).

Ranz, W. E., ''Fluid Mechanical Mixing-Lamellar Description,'' *Mixing of Liquids by Mechanical Agitation*, J. J. Ulbrecht and G. K. Patterson, eds., Gordon and Breach, New York, p. 1 (1985).

Russ, J. C., *The Image Processing Handbook*, 2nd ed., CRC Press, Boca Raton (1994).

Strang, G., and T. Nguyen, *Wavelets and Filter Banks*, Wesley-Cambridge Press, Wellesley, MA (1997).

Wei, J., ''The Multiscale Structure of Uniformity in Mixtures,'' *I&EC Res.*, **38**, 576 (1999).

Manuscript received Nov. 17, 1998, and revision received June 10, 1999.